



Discovery of novel dual PPAR α / δ agonists based on benzimidazole scaffold for the treatment of non-alcoholic fatty liver disease

Zheng Li^{a,b,*}, Yawen Xu^a, Zongyu Cai^a, Xuekun Wang^c, Qiang Ren^a, Zongtao Zhou^a, Rongrong Xie^{a,*}

^a School of Pharmacy, Guangdong Pharmaceutical University, Guangzhou 510006, PR China

^b Key Laboratory of New Drug Discovery and Evaluation of Ordinary Universities of Guangdong Province, Guangdong Pharmaceutical University, Guangzhou 510006, PR China

^c College of Pharmacy, Liaocheng University, Liaocheng 252059, PR China

ARTICLE INFO

Keywords:

Dual agonist
Fatty liver
Fibrosis
NASH
PPAR

ABSTRACT

Many peroxisome proliferator-activated receptors (PPARs) agonists have been developed for the treatment of metabolic disorders, while several PPARs agonists were discontinued in clinical trials because of PPAR γ related side effects. In order to increase the selectivity against PPAR γ , we performed a structure-activity relationship study based on PPAR α / γ / δ agonist MHY2013. These efforts eventually led to the identification of compound **4**, a dual PPAR α / δ agonist with considerable potencies on PPAR α / δ and high selectivity against PPAR γ . In the Western Diet and CCl₄-induced non-alcoholic steatohepatitis model, compound **4** alleviates the hepatic steatosis, inflammation, and fibrosis. These results indicated that dual PPAR α / δ agonist **4** might be a promising lead compound for further investigations.

1. Introduction

Non-alcoholic fatty liver disease (NAFLD) is one of the most prevalent liver diseases, which includes different course of the disease, from hepatic steatosis to non-alcoholic steatohepatitis (NASH) followed by fibrosis [1,2]. Although various factors including obesity, insulin resistance and inflammation have been attributed to the development of NAFLD, the exact pathogenesis is still unclear [3,4]. To date, there are no approved drugs for NAFLD [5,6].

The peroxisome proliferator-activated receptors (PPARs), including PPAR α / δ / γ , have an important role in energy metabolism [7–9]. PPAR α is primarily expressed in the liver and modulates plasma lipid levels, fatty acid β -oxidation and transport [10–12]. PPAR δ is primarily expressed in muscle tissue, which modulates fatty acid transport and β -oxidation [13,14]. Moreover, the activation of PPAR δ improves plasma lipid levels and insulin sensitivity, and provides anti-inflammatory effects [15–17]. PPAR γ is primarily expressed in adipocytes, which increases the storage of fatty acids and improves insulin resistance [18]. At present, many PPARs agonists (Fig. 1) have been developed for the treatment of dyslipidemia, NAFLD and diabetes [19–21]. In our previous study, we have also discovered several PPAR δ agonists with a therapeutic effect on glucose and lipid metabolism [22–24]. Although the field is promising, several PPARs agonists were discontinued in

clinical trials because of PPAR γ related side effects such as weight gain, fluid retention, and cardiovascular risk [25,26]. As a potent PPAR α / γ / δ agonist, MHY2013 reduces insulin resistance, plasma lipid level and hepatic steatosis [27]. In order to decrease the risk of PPAR γ related side effects, a lot of research has been done to obtain dual PPAR α / δ agonist. Herein, we describe the structure-activity relationship study based on MHY2013 to further increase selectivity against PPAR γ (Fig. 2).

2. Results and discussion

2.1. Chemistry

The designed compounds **1–12** were synthesized as shown in Scheme 1. Treatment of commercially available **B** with phenol **A** using Williamson ether synthesis provided intermediate **C**, which was converted into benzimidazole with good yields [28], followed by hydrolysis provided the target compounds **1–12**.

2.2. Structure-activity relationship study

In vitro activities of target compounds on PPAR α / γ / δ were evaluated by using cell-based assays. As shown in Table 1, replacing

* Corresponding authors at: School of Pharmacy, Guangdong Pharmaceutical University, Guangzhou 510006, PR China (Z. Li).

E-mail addresses: li.zheng.sky@163.com (Z. Li), happyyunyun_1985@126.com (R. Xie).

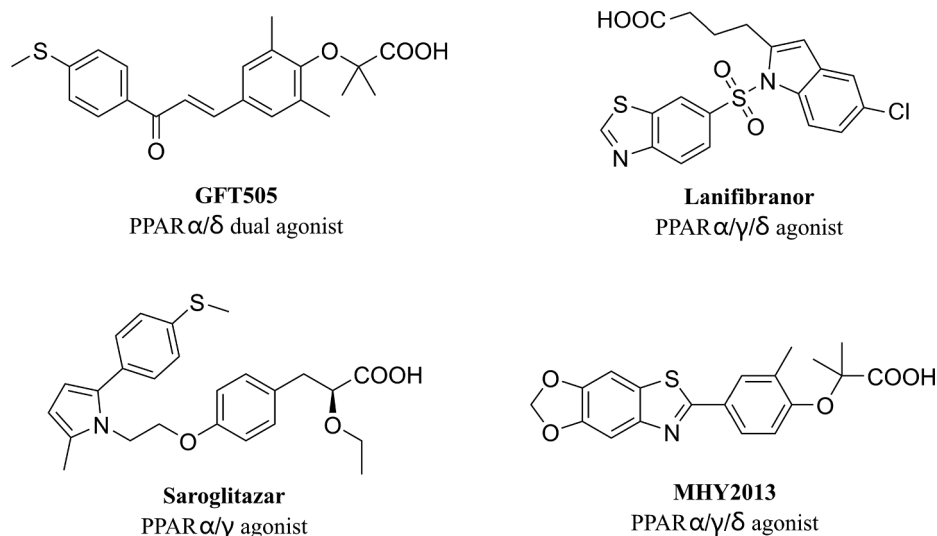


Fig. 1. Structure of representative PPAR α , PPAR γ and PPAR δ agonists.

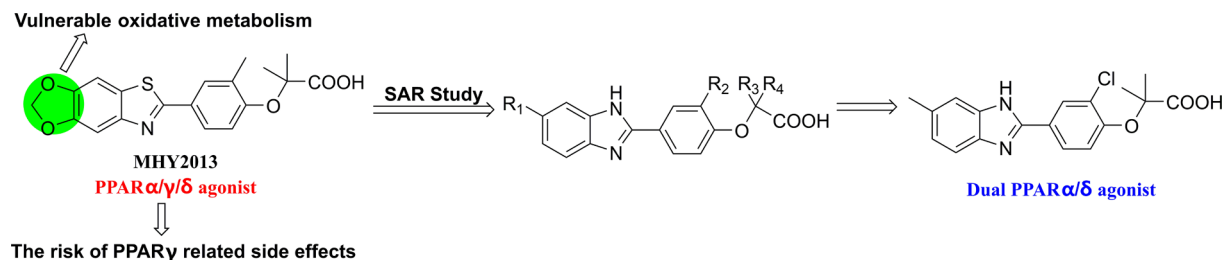
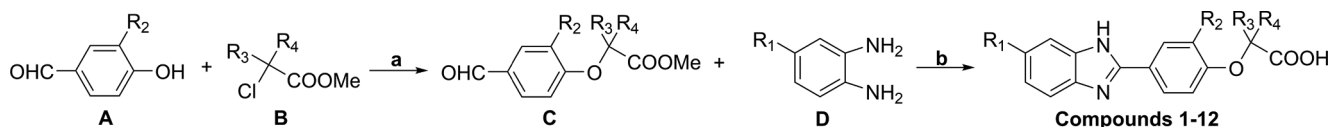


Fig. 2. Our design strategy and structure-activity relationship study to obtain dual PPAR α/δ agonist from PPAR $\alpha/\gamma/\delta$ agonist MHY2013.



Scheme 1. Synthesis of target compounds 1–11. Reagents and conditions: (a) K_2CO_3 , acetonitrile, 45 °C, 12 h; (b) H_2O (10 vol% in DMF), 80 °C, open flask, and then $LiOH \cdot H_2O$, THF/MeOH/ H_2O , r.t., 4 h.

Table 1

Compd.	In vitro activities of target compounds on PPAR $\alpha/\delta/\gamma$				EC ₅₀ (nM)		
	R ₁	R ₂	R ₃	R ₄	PPAR α ^a	PPAR γ	PPAR δ
MHY2013					217	185	163
1	Me	Me	Me	Me	349	736	278
2	CF ₃	Me	Me	Me	385	684	296
3	Cl	Me	Me	Me	481	1075	451
4	Me	Cl	Me	Me	307	2052	214
5	Me	F	Me	Me	891	2839	1035
6	H	Me	Me	H	953	2571	717
7	CF ₃	Me	Me	H	579	2137	341
8	Me	Me	H	H	1035	3124	848
9	Cl	Me	H	H	1479	4016	1327
10	CF ₃	Me	H	H	1437	3363	1206
11	Me	F	H	H	3725	5932	1507
12	Me	Cl	H	H	859	3769	684

^a EC₅₀ value represents the mean of three determinations.

benzothiazole of MHY2013 with benzimidazole provided compound 1 with decreased activities on PPAR $\alpha/\gamma/\delta$, while increasing selectivity against PPAR γ . Indeed, the benzimidazole scaffold has been widely

reported in PPAR modulators [29–31]. Exploration of other hydrophobic substituents (CF₃ and Cl) at the benzimidazole scaffold provided compounds 2 and 3, which have less effect on the selectivity against PPAR γ . Notably, replacing methyl at right benzene with chlorine afforded compound 4, which revealed better activities on PPAR α/δ and higher selectivity against PPAR γ compared to parent compound 1. Further replacement with fluorine (compound 5) significantly decreased potencies on PPAR $\alpha/\gamma/\delta$, indicating that hydrophobic interaction in this site might be crucial to agonistic activity. Next, we explored the importance of carboxylic acid moiety. Removing a methyl group in acid moiety reduced activity on PPAR $\alpha/\gamma/\delta$ (compounds 6 and 7), but enhanced selectivity against PPAR γ (compound 7 vs 2). The structure-activity relationship of phenoxy acetic acid series (compounds 8–12) was also explored, while both of them revealed lower potencies on PPAR $\alpha/\gamma/\delta$ compared to their parent compounds (compound 8 vs 1, 9 vs 3, 10 vs 2, 11 vs 5, and 12 vs 4). Among all of these compounds, the optimal compound 4 revealed the best agonistic activity on PPAR α/δ and high selectivity against PPAR γ .

2.3. Docking study

To better understand the binding model of compound 4, we performed the modeling studies based on the complex structures of PPAR α (PDB code: 3V18) and PPAR δ (PDB code: 1GWX). As shown in Fig. 3,

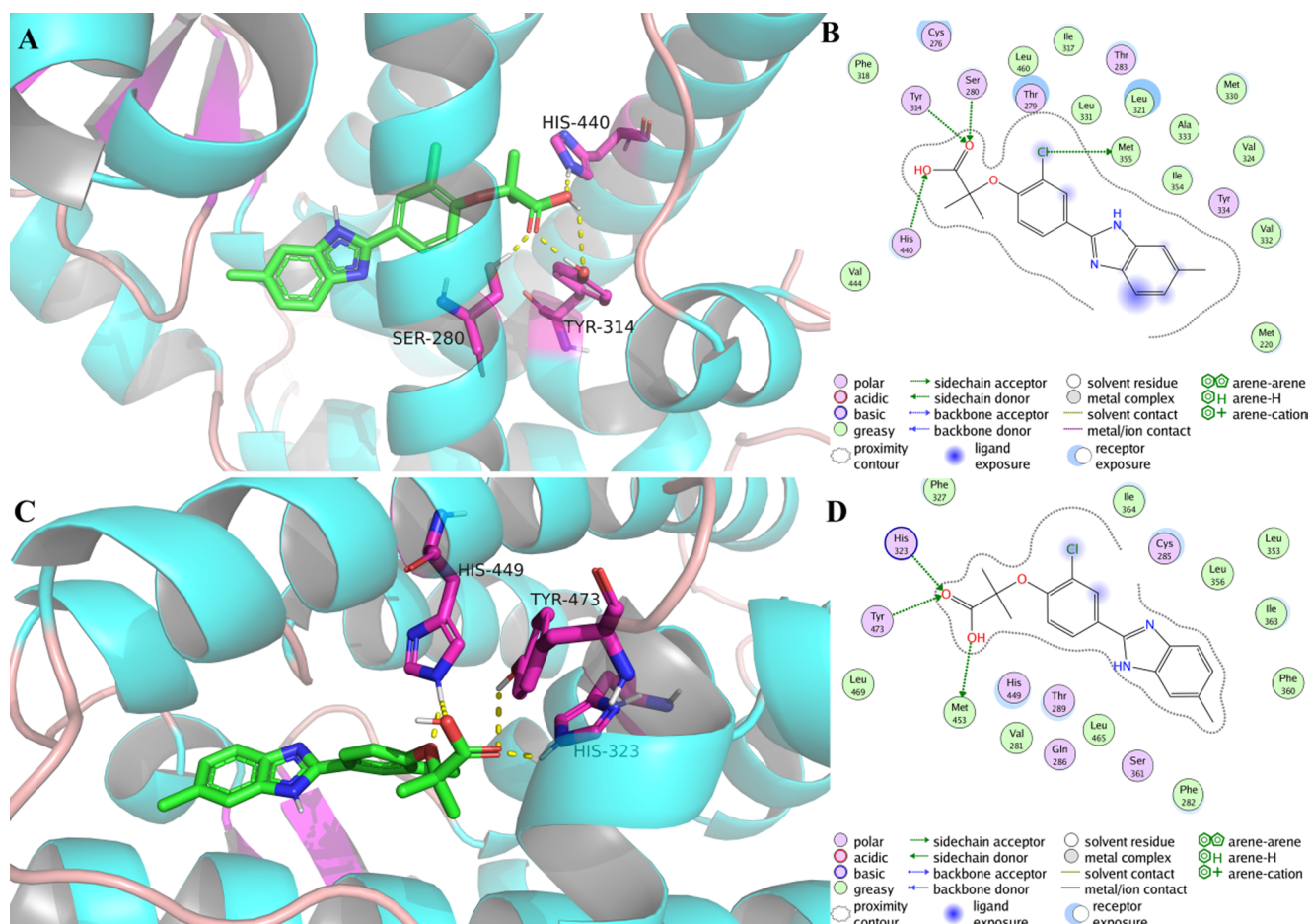


Fig. 3. The 3-D binding diagram (A) and 2-D interaction map (B) of compound **4** (green carbon) in the crystal structure of PPAR α (3VI8), and 3-D binding diagram (C) and 2-D interaction map (D) of compound **4** (green carbon) in the crystal structure of PPAR δ (1GWX). Key residues are labeled, and interactions are represented by yellow dashed lines. (For interpretation of the references to colour in this figure legend, the reader is referred to the web version of this article.)

compound **4** fitted very well with the binding pocket of PPAR α and PPAR δ . The carboxylic acid of compound **4** generated hydrogen-bonding interactions with His440, Tyr314, and Ser280 in the binding pocket of PPAR α (Fig. 3A and B). Moreover, the benzimidazole scaffold of compound **4** is inserted into the hydrophobic pocket of PPAR α . The binding mode of compound **4** in PPAR δ is slightly different from PPAR α , which exhibited a rotation angle between benzimidazole and the right hand benzene of compound **4** (Fig. 3C). The carboxylic acid of compound **4** formed three hydrogen-bonding with His449, Tyr473 and His323. Moreover, hydrogen-bonding was also generated between the oxygen atom of compound **4** and His449.

2.4. Effects on fatty liver

The effects of compound **4** on the fatty liver were evaluated in WD/CCL₄ mice, a Western Diet and CCL₄-induced NASH model [32]. As shown in Fig. 4, the hepatic steatosis and inflammation were significantly increased WD/CCL₄ mice, which were alleviated in MHY2013 and compound **4** groups. Plasma levels of AST and ALT, the markers of hepatic injury, were raised in WD/CCL₄ mice compared to normal mice. Similar to the improvement of fatty liver, AST and ALT levels were notably diminished by the treatment of compound **4** (Fig. 4). Moreover, liver fibrosis induced by the Western Diet and CCL₄ was also ameliorated in compound **4**-treated group (Fig. 5). These results indicated that compound **4** might be a promising dual PPAR α/δ agonist for the treatment of fatty liver.

3. Conclusion

In order to decrease the risk of PPAR γ related side effects, we performed a structure-activity relationship study based on PPAR $\alpha/\gamma/\delta$ agonist MHY2013. All of these efforts resulted in the discovery of dual PPAR α/δ agonist **4**, which revealed the best agonistic activity on PPAR α/δ and high selectivity against PPAR γ in our researches. Further modeling studies illuminated that compound **4** fitted very well with the binding pocket of PPAR α and PPAR δ , and formed multiple interactions with key residues related to the agonistic activity. Moreover, the hepatic steatosis, inflammation, and fibrosis were significantly alleviated in the NASH model after treated with compound **4**. In summary, we described the discovery process of novel dual PPAR α/δ agonists, and compound **4** was identified as a promising lead compound for further researches.

4. Experimental section

4.1. General chemistry

All starting materials, reagents, and solvents were obtained from commercial sources. Purifications of chromatography were performed by silica gel and detected by thin layer chromatography using UV light at 254 and 365 nm. Melting points were measured on RY-1 melting-point apparatus. NMR spectra were recorded on a Bruker ACF-300Q instrument (300 MHz for ¹H NMR and 75 MHz for ¹³C NMR spectra), chemical shifts are expressed as values (ppm) relative to

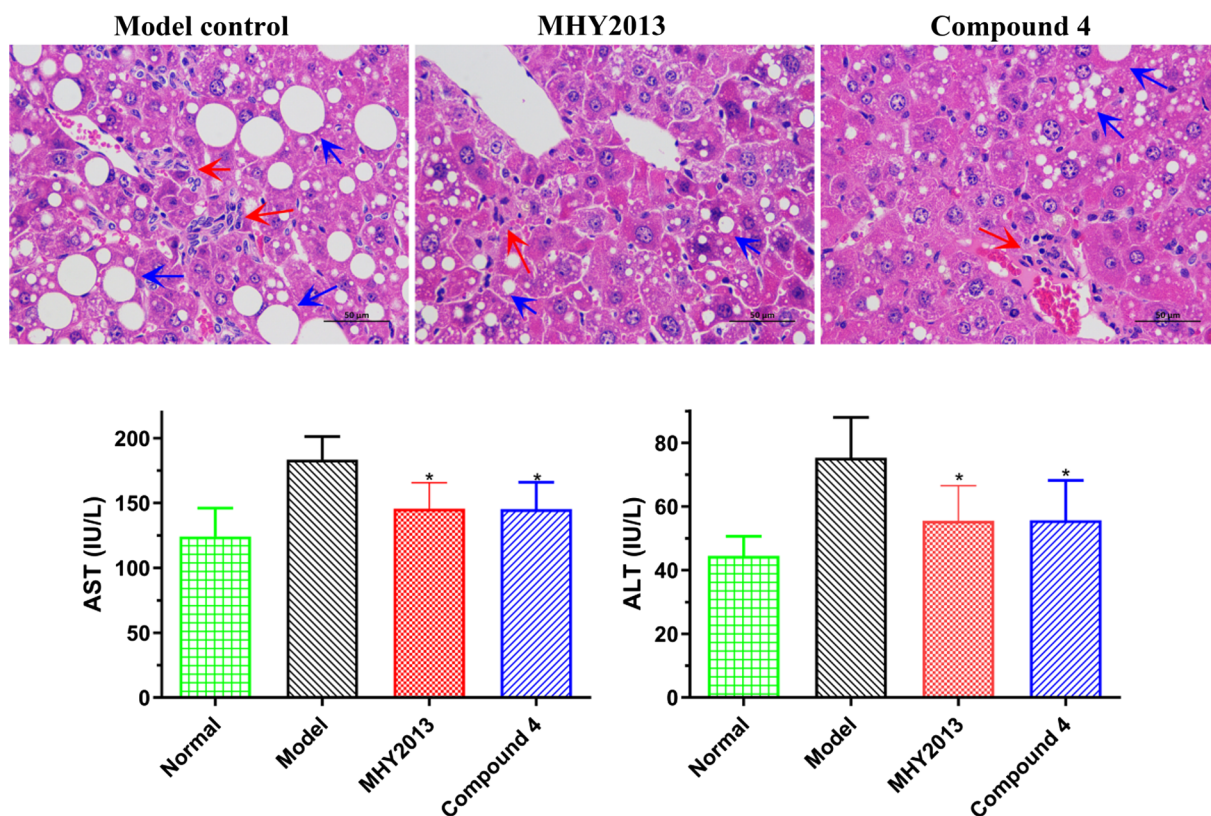


Fig. 4. Effect of compound 4 on the fatty liver after 30 days of treatment in WD/CCL₄ mice. Representative photomicrographs of histological alterations in liver stained with Hematoxylin-Eosin at 400× magnification. Empty/hollow spaces show fat globules or accumulation (macro-vesicular steatosis). Steatosis: blue arrow, inflammation: red arrow. Histograms show the plasma levels of Aspartate transaminase (AST) and Alanine transaminase (ALT). All the values are expressed as mean ± SD (n = 6). **p* ≤ 0.05 compared to model control were analyzed using a one-way ANOVA with Tukey's multiple-comparison post hoc test. (For interpretation of the references to colour in this figure legend, the reader is referred to the web version of this article.)

tetramethylsilane as internal standard, and coupling constants (*J* values) were given in hertz (Hz). LC/MS spectra were recorded on a Waters LC-MS system (ESI). Elemental analyses were performed by the Heraeus CHN-O-Rapid analyzer and were within 0.4% of the theoretical values. MHY2013 was synthesized by published procedures [27].

4.1.1. General synthetic procedure for target compounds 1–12

To a stirred solution of **A** (1 equiv) in acetonitrile was added potassium carbonate (3 equiv) and **B** (2 equiv). The mixture was stirred at 45 °C for 12 h, and filtered. The filtrate was concentrated and the residue was dissolved in ethyl acetate. The organic layers were washed with brine (2 × 20 mL), dried over anhydrous sodium sulfate and filtered. The filtrate was concentrated to give intermediate **C**, which was used for the next reaction without further purification. The intermediate **C** (1.0 equiv) and **D** (1.0 equiv) were dissolved in DMF (90 vol % in H₂O). The resulting reaction mixture was stirred at 80 °C in an

open flask, and the reaction progress was monitored by TLC. Then the reaction mixture was poured into water (60 mL) and extracted with ethyl acetate (3 × 25 mL). The combined organic phases were washed with water (25 mL), dried over anhydrous sodium sulfate and filtered. The filtrate was evaporated and the residue was purified by silica gel column chromatography (petroleum ether/ethyl acetate, 10:1, v/v). To a solution of the obtained solid (1 equiv) in 2:3:1 THF/MeOH/H₂O (18 mL) was added LiOH·H₂O (3 equiv). After stirring at room temperature for 4 h, the volatiles were removed under reduced pressure. The residue was acidified with 1 N hydrochloric acid solution and then filtered and the filter cake was washed with 5 mL of water, dried in vacuum to afford a white powder. The white powder was purified by column chromatography using a mixture of petroleum ether/ethyl acetate (2:1–1:2, v/v) as eluent to afford the target compounds as solid.

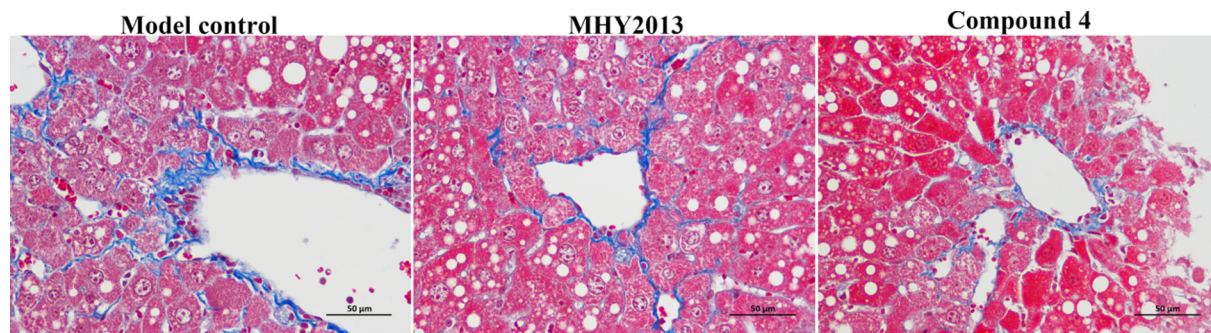


Fig. 5. Effect of compound 4 on liver fibrosis (Masson's trichrome staining) of WD/CCL₄ mice.

4.1.2. 2-Methyl-2-(2-methyl-4-(6-methyl-1H-benzo[d]imidazol-2-yl)phenoxy)propanoic acid (1)

Yield 32%; melting point, 247–249 °C; ¹H NMR (300 MHz, D₂O) δ: 10.53–10.29 (m, 2H), 9.87 (d, *J* = 8.4 Hz, 1H), 9.77 (s, 1H), 9.56–9.47 (m, 1H), 9.10 (d, *J* = 8.7 Hz, 1H), 5.38 (s, 1H), 4.70 (s, 3H), 4.49 (s, 3H), 3.85 (s, 6H). ¹³C NMR (75 MHz, DMSO-*d*₆) δ: 174.89, 158.54, 151.73, 135.12, 132.69, 131.45, 129.69, 128.05, 126.43, 125.65, 122.25, 115.73, 115.38, 114.69, 79.65, 25.63, 21.35, 16.76. ESI-MS *m/z*: 323.1 [M–H][−]. Anal. calcd. For C₁₉H₂₀N₂O₃: C, 70.35; H, 6.21; N, 8.64; Found: C, 70.46; H, 6.33; N, 8.72.

4.1.3. 2-Methyl-2-(2-methyl-4-(6-(trifluoromethyl)-1H-benzo[d]imidazol-2-yl)phenoxy)propanoic acid (2)

Yield 37%; melting point, 230 °C (carbonize); ¹H NMR (300 MHz, D₂O) δ: 10.67–10.44 (m, 2H), 10.26 (s, 1H), 10.17 (d, *J* = 8.5 Hz, 1H), 10.00 (d, *J* = 8.5 Hz, 1H), 9.09 (d, *J* = 8.7 Hz, 1H), 5.37 (s, 1H), 4.47 (s, 3H), 3.84 (s, 6H). ¹³C NMR (75 MHz, DMSO-*d*₆) δ: 174.87, 158.57, 151.79, 135.46, 132.90, 131.31, 129.53, 128.01, 126.47, 126.05, 125.62, 122.27, 115.79, 115.35, 111.67, 79.69, 25.60, 16.82. ESI-MS *m/z*: 377.1 [M–H][−]. Anal. calcd. For C₁₉H₁₇F₃N₂O₃: C, 60.32; H, 4.53; N, 7.40; Found: C, 60.15; H, 4.38; N, 7.52.

4.1.4. 2-(4-(6-Chloro-1H-benzo[d]imidazol-2-yl)-2-methylphenoxy)-2-methylpropanoic acid (3)

Yield 34%; melting point, 248 °C (carbonize); ¹H NMR (300 MHz, DMSO-*d*₆) δ: 8.26 (d, *J* = 1.6 Hz, 1H), 8.19 (dd, *J* = 8.7, 2.1 Hz, 1H), 7.80–7.70 (m, 2H), 7.46, 7.43 (dd, *J* = 8.7, 1.9 Hz, 1H), 6.86 (d, *J* = 8.7 Hz, 1H), 2.26 (s, 3H), 1.62 (s, 6H). ¹³C NMR (75 MHz, DMSO-*d*₆) δ: 174.98, 157.94, 150.87, 134.98, 132.87, 130.89, 129.43, 129.33, 127.39, 125.38, 117.00, 115.76, 115.60, 114.05, 79.57, 25.62, 16.87. ESI-MS *m/z*: 343.1 [M–H][−]. Anal. calcd. For C₁₈H₁₇ClN₂O₃: C, 62.70; H, 4.97; N, 8.12; Found: C, 62.79; H, 4.89; N, 8.07.

4.1.5. 2-(2-Chloro-4-(6-methyl-1H-benzo[d]imidazol-2-yl)phenoxy)-2-methylpropanoic acid (4)

Yield 27%; melting point, 250 °C (carbonize); ¹H NMR (300 MHz, DMSO-*d*₆) δ: 8.59 (d, *J* = 2.1 Hz, 1H), 8.35 (dd, *J* = 8.8, 2.1 Hz, 1H), 7.64 (d, *J* = 8.3 Hz, 1H), 7.54 (s, 1H), 7.28 (d, *J* = 8.4 Hz, 1H), 7.08 (d, *J* = 8.8 Hz, 1H), 2.45 (s, 3H), 1.65 (s, 6H). ¹³C NMR (75 MHz, DMSO-*d*₆) δ: 174.32, 154.83, 147.57, 135.63, 133.42, 131.43, 130.15, 128.18, 127.22, 124.78, 118.42, 117.95, 114.07, 113.80, 81.08, 25.50, 21.65. ESI-MS *m/z*: 343.1 [M–H][−]. Anal. calcd. For C₁₈H₁₇ClN₂O₃: C, 62.70; H, 4.97; N, 8.12; Found: C, 62.56; H, 4.85; N, 8.23.

4.1.6. 2-(2-Fluoro-4-(6-methyl-1H-benzo[d]imidazol-2-yl)phenoxy)-2-methylpropanoic acid (5)

Yield 29%; melting point, 217–218 °C; ¹H NMR (300 MHz, D₂O) δ: 10.74–10.57 (m, 1H), 10.44 (d, *J* = 8.7 Hz, 1H), 9.89 (d, *J* = 8.4 Hz, 1H), 9.80 (s, 1H), 9.56 (d, *J* = 8.4 Hz, 1H), 9.38 (t, *J* = 8.6 Hz, 1H), 5.37 (s, 1H), 4.69 (s, 3H), 3.85 (s, 6H). ¹³C NMR (75 MHz, DMSO-*d*₆) δ: 174.23, 147.62, 147.38, 136.27, 132.54, 130.41, 127.75, 125.41, 119.85, 116.52, 113.90, 113.69, 81.16, 25.43, 21.64. ESI-MS *m/z*: 327.1 [M–H][−]. Anal. calcd. For C₁₈H₁₇FN₂O₃: C, 65.85; H, 5.22; N, 8.53; Found: C, 65.67; H, 5.35; N, 8.58.

4.1.7. 2-(4-(1H-Benzo[d]imidazol-2-yl)-2-methylphenoxy)propanoic acid (6)

Yield 25%; melting point, 241 °C (carbonize); ¹H NMR (300 MHz, DMSO-*d*₆) δ 13.24 (s, 1H), 8.23–8.00 (m, 2H), 7.77–7.72 (m, 2H), 7.46–7.41 (m, 2H), 7.09 (d, *J* = 8.7 Hz, 1H), 5.08 (q, *J* = 6.8 Hz, 1H), 2.31 (s, 3H), 1.60 (d, *J* = 6.8 Hz, 3H). ¹³C NMR (75 MHz, DMSO-*d*₆) δ: 173.07, 159.42, 150.05, 135.35, 131.35, 130.37, 127.81, 127.56, 125.00, 114.46, 112.87, 72.34, 18.72, 16.64. ESI-MS *m/z*: 295.1 [M–H][−]. Anal. calcd. For C₁₇H₁₆N₂O₃: C, 68.91; H, 5.44; N, 9.45; Found: C, 68.73; H, 5.58; N, 9.33.

4.1.8. 2-(2-Methyl-4-(6-(trifluoromethyl)-1H-benzo[d]imidazol-2-yl)phenoxy)propanoic acid (7)

Yield 31%; melting point, 235 °C (carbonize); ¹H NMR (300 MHz, DMSO-*d*₆) δ 13.38 (s, 1H), 8.25–8.02 (m, 2H), 8.04 (d, *J* = 6.0 Hz, 1H), 7.98–7.93 (m, 1H), 7.77–7.72 (m, 1H), 7.09 (d, *J* = 8.5 Hz, 1H), 5.09 (q, *J* = 6.8 Hz, 1H), 2.31 (s, 3H), 1.59 (d, *J* = 6.8 Hz, 3H). ¹³C NMR (75 MHz, DMSO-*d*₆) δ: 174.78, 158.57, 151.68, 135.76, 132.59, 131.62, 129.37, 128.12, 126.35, 126.18, 125.27, 122.29, 115.53, 115.47, 111.58, 65.69, 18.74, 16.65. ESI-MS *m/z*: 363.1 [M–H][−]. Anal. calcd. For C₁₈H₁₅F₃N₂O₃: C, 59.34; H, 4.15; N, 7.69; Found: C, 59.15; H, 4.07; N, 7.56.

4.1.9. 2-(2-Methyl-4-(6-methyl-1H-benzo[d]imidazol-2-yl)phenoxy)acetic acid (8)

Yield 45%; melting point, 254–256 °C; ¹H NMR (300 MHz, DMSO-*d*₆) δ 8.28–8.16 (m, 2H), 8.05 (s, 1H), 7.95 (d, *J* = 8.5 Hz, 1H), 7.78 (dd, *J* = 8.7, 1.8 Hz, 1H), 7.19 (d, *J* = 8.5 Hz, 1H), 4.91 (s, 2H), 2.32 (s, 3H), 2.26 (s, 3H). ¹³C NMR (75 MHz, DMSO-*d*₆) δ: 174.62, 158.38, 151.51, 135.30, 132.21, 131.35, 129.43, 128.01, 126.55, 125.46, 122.12, 115.65, 115.34, 114.58, 65.75, 21.65, 16.76. ESI-MS *m/z*: 295.1 [M–H][−]. Anal. calcd. For C₁₇H₁₆N₂O₃: C, 68.91; H, 5.44; N, 9.45; Found: C, 68.78; H, 5.35; N, 9.38.

4.1.10. 2-(4-(6-Chloro-1H-benzo[d]imidazol-2-yl)-2-methylphenoxy)acetic acid (9)

Yield 42%; melting point, 276–278 °C; ¹H NMR (300 MHz, DMSO-*d*₆) δ: 8.27 (d, *J* = 1.8 Hz, 1H), 8.21 (dd, *J* = 8.6, 2.2 Hz, 1H), 7.82–7.74 (m, 2H), 7.45, 7.42 (dd, *J* = 8.8, 1.8 Hz, 1H), 6.88 (d, *J* = 8.8 Hz, 1H), 4.60 (s, 2H), 2.25 (s, 3H). ¹³C NMR (75 MHz, DMSO-*d*₆) δ: 174.87, 157.96, 150.85, 134.96, 132.85, 130.87, 129.46, 129.37, 127.35, 125.39, 117.03, 115.78, 115.62, 114.03, 65.77, 16.81. ESI-MS *m/z*: 315.1 [M–H][−]. Anal. calcd. For C₁₆H₁₃ClN₂O₃: C, 60.67; H, 4.14; N, 8.84; Found: C, 60.48; H, 4.07; N, 8.68.

4.1.11. 2-(2-Methyl-4-(6-(trifluoromethyl)-1H-benzo[d]imidazol-2-yl)phenoxy)acetic acid (10)

Yield 47%; melting point, 221–223 °C; ¹H NMR (300 MHz, DMSO-*d*₆) δ 12.57 (s, 1H), 7.99 (d, *J* = 2.3 Hz, 1H), 7.91 (dd, *J* = 8.5, 2.3 Hz, 1H), 7.39–7.33 (m, 2H), 7.05–7.00 (m, 2H), 4.91 (s, 2H), 2.30 (s, 3H). ¹³C NMR (75 MHz, DMSO-*d*₆) δ: 174.73, 158.55, 151.76, 135.43, 132.82, 131.35, 129.34, 128.07, 126.23, 126.12, 125.56, 122.38, 115.68, 115.32, 111.65, 65.64, 16.82. ESI-MS *m/z*: 349.1 [M–H][−]. Anal. calcd. For C₁₇H₁₃F₃N₂O₃: C, 58.29; H, 3.74; N, 8.00; Found: C, 58.12; H, 3.63; N, 8.09.

4.1.12. 2-(2-Fluoro-4-(6-methyl-1H-benzo[d]imidazol-2-yl)phenoxy)acetic acid (11)

Yield 43%; melting point, 196–198 °C; ¹H NMR (300 MHz, DMSO-*d*₆) δ 12.39 (s, 1H), 8.22 (d, *J* = 2.2 Hz, 1H), 8.06 (dd, *J* = 8.7, 2.2 Hz, 1H), 7.46 (d, *J* = 8.2 Hz, 1H), 7.36 (s, 1H), 7.22 (d, *J* = 8.7 Hz, 1H), 7.02 (dd, *J* = 8.2, 1.6 Hz, 1H), 4.92 (s, 2H), 2.42 (s, 3H). ¹³C NMR (75 MHz, DMSO-*d*₆) δ: 174.63, 157.45, 149.93, 135.15, 132.73, 131.15, 125.95, 125.71, 124.65, 117.01, 115.35, 115.12, 114.32, 65.73, 21.65. ESI-MS *m/z*: 299.1 [M–H][−]. Anal. calcd. For C₁₆H₁₃FN₂O₃: C, 64.00; H, 4.36; N, 9.33; Found: C, 64.21; H, 4.23; N, 9.18.

4.1.13. 2-(2-Chloro-4-(6-methyl-1H-benzo[d]imidazol-2-yl)phenoxy)acetic acid (12)

Yield 38%; melting point, 243–245 °C; ¹H NMR (300 MHz, DMSO-*d*₆) δ 13.44 (s, 1H), 8.47 (d, *J* = 2.3 Hz, 1H), 8.28 (dd, *J* = 8.8, 2.3 Hz, 1H), 7.65 (d, *J* = 8.3 Hz, 1H), 7.55 (s, 1H), 7.39 (d, *J* = 8.8 Hz, 1H), 7.32–7.28 (m, 1H), 5.01 (s, 2H), 2.48 (s, 3H). ¹³C NMR (75 MHz, DMSO-*d*₆) δ: 174.42, 157.45, 149.93, 135.13, 132.55, 131.95, 128.45, 125.83, 123.42, 116.25, 115.32, 115.16, 65.75, 21.63. ESI-MS *m/z*: 315.1 [M–H][−]. Anal. calcd. For C₁₆H₁₃ClN₂O₃: C, 60.67; H, 4.14; N, 8.84; Found: C, 60.52; H, 4.05; N, 8.71.

4.2. Evaluation for PPAR α , PPAR γ and PPAR δ

Detailed descriptions on transfection and cell-based evaluation for PPAR α , PPAR γ , and PPAR δ were given in our previously reported literature [22]. Briefly, HepG2 or HEK293 cells were transfected with pBIND-PPAR α , PPAR δ or PPAR γ according to the manufacturer's protocol. After transfection, positive controls or compounds with different concentrations were added and incubated for 18 h, then lysed with lysis buffer, and added Luciferase Assay Reagent II. The luciferase signals of firefly and renilla were measured using Dual Luciferase Reporter Assay System (Promega). EC₅₀ values were obtained from GraphPad 5.00 (San Diego, USA).

4.3. Molecular modeling

MOE (version 2014.0901, The Chemical Computing Group, Montreal, Canada) was used to perform the docking modeling based on the reported crystal structure of PPAR α (3V18) and PPAR δ (1GWX). Prior to molecular docking, other crystallized ligands and water were removed, and the obtained protein was performed by Protonate 3D prior to the Gaussian Contact surface was draw around the binding pocket. Subsequently, the binding pocket with the Gaussian Contact surface was isolated and the backbone was deleted. The ligand poses in binding site was filtered by using Pharmacophore Query Editor. Compound 4 was docked into the binding pocket with the Pharmacophore method and ranked with London dG scoring function. For energy minimization in the binding pocket, MOE Forcefield Refinement was performed and ranked with London dG scoring function. All protocols were validated by re-docking of the crystal ligands into the binding pocket of PPAR α and PPAR δ . The RMSD between the co-crystal ligand and the performed experiment must be less than 2.0 Å in all cases (0.85 Å and 1.56 Å, respectively). These values indicate that the parameters used for calculations agree by replicating the conformation and orientation in the X-ray coordinates of the receptors. MOE 2014.0901 and Pymol 2.3 were employed for adequate visualization.

4.4. Animals

8 weeks old male C57BL/6J mice were purchased from Guangdong Medical Laboratory Animal Center (Guangdong, China), and mice were acclimatized for one week. The animal room was maintained relative humidity 50 ± 10% at 23 ± 2 °C under 12 h light/black throughout the experimental period. Food and water were allowed ad libitum access for animals unless otherwise stated, and 0.5% Carboxy Methyl Cellulose solution was used as vehicle for drug administration. The ethical committee of Guangdong Pharmaceutical University has approved all experimental procedures involved in animals, and these experimental procedures were performed based on Laboratory Animal Management Regulations in China and adhered to the Guide for the Care and Use of Laboratory Animals (NIH publication, 2011).

4.5. Effects of compound 4 on fatty liver

Mice were fed a normal chow Diet and normal tap water as normal control. NASH model was induced by Western Diet (WD) containing 21.1% fat, 41% Sucrose, and 1.25% Cholesterol by weight and a high sugar solution (23.1 g/L fructose and 18.9 g/L glucose). CCl₄ in corn oil at the dose of 0.2 μl/g of body weight was injected intra-peritoneally once/week for 12 weeks, starting simultaneously with the Western Diet administration. In the ninth week, the WD/CCl₄ mice were dosed once daily with the vehicle, HMY2013 (20 mg/kg), or compound 4 (20 mg/kg) by gavage administration for 4 weeks (n = 6 per group). Mice were dosed at a fixed time daily. The body weights were measured every 5 days and the dosage was adjusted according to the most recent body weight. At the end of treatment, mice were euthanized by

exsanguination after ketamine and xylazine anesthesia. Tissue and serum samples were collected and processed for histological and serological analysis. Alanine aminotransferase (ALT) and aspartate transaminase (AST) levels were determined by the automatic biochemical analyzer (Beckman Coulter, AU5811, Tokyo, Japan). The liver of each experimental group was isolated immediately after sacrifice and washed with ice-cold saline before fixed in 10% (v/v) formalin. The sections were embedded in paraffin after dehydrate. Four-micron sections were cut and stained with Hematoxylin-Eosin and Masson's trichrome staining for histopathological assessment at 400 × magnification.

Declaration of Competing Interest

The authors declare no competing financial interest.

Acknowledgments

This study was supported by the Natural Science Foundation of Guangdong Province, China (Grant 2018A030313445), the Guangdong Basic and Applied Basic Research Foundation, China (Grant 2019A1515011036), the Innovative strong school project of Guangdong Pharmaceutical University, China (Grant 2018KTSCX111), Guangdong Province Medical Science and Technology Research Fund, China (Grant B2018053), and Research Projects of the Chinese Medicine Council of Guangdong Province, China (Grant 20191199 and 20192043).

References

- [1] M.E. Rinella, Nonalcoholic fatty liver disease: a systematic review, *JAMA* 313 (2015) 2263–2273.
- [2] R.J. Wong, M. Aguilar, R. Cheung, R.B. Perumpail, S.A. Harrison, Z.M. Younossi, A. Ahmed, Nonalcoholic steatohepatitis is the second leading etiology of liver disease among adults awaiting liver transplantation in the United States, *Gastroenterology* 148 (2015) 547–555.
- [3] J.H. Huh, K.J. Kim, S.U. Kim, S.H. Han, K.H. Han, B.S. Cha, C.H. Chung, B.W. Lee, Obesity is more closely related with hepatic steatosis and fibrosis measured by transient elastography than metabolic health status, *Metabolism* 66 (2017) 23–31.
- [4] M. Noureddin, A.J. Sanyal, Pathogenesis of NASH: the impact of multiple pathways, *Curr. Hepatol. Rep.* 17 (2018) 350–360.
- [5] Z.M. Younossi, R. Loomba, M.E. Rinella, E. Bugianesi, G. Marchesini, B.A. Neuschwander-Tetri, L. Serfaty, F. Negro, S.H. Caldwell, V. Ratzliff, K.E. Corey, S.L. Friedman, M.F. Abdelmalek, S.A. Harrison, A.J. Sanyal, J.E. Lavine, P. Mathurin, M.R. Charlton, N.P. Chalasani, Q.M. Anstee, K.V. Kowdley, J. George, Z.D. Goodman, K. Lindor, Current and future therapeutic regimens for nonalcoholic fatty liver disease and nonalcoholic steatohepatitis, *Hepatology* (Baltimore, Md.) 68 (2018) 361–371.
- [6] Y. Sumida, M. Yoneda, Current and future pharmacological therapies for NAFLD/ NASH, *J. Gastroenterol.* 53 (2018) 362–376.
- [7] Z.-H. Zhao, Y.-C. Fan, Q. Zhao, C.-Y. Dou, X.-F. Ji, J. Zhao, S. Gao, X.-Y. Li, K. Wang, Promoter methylation status and expression of PPAR-gamma gene are associated with prognosis of acute-on-chronic hepatitis B liver failure, *Clin. Epigenet* 7 (2015).
- [8] F. Hong, S. Pan, Y. Guo, P. Xu, Y. Zhai, PPARs as nuclear receptors for nutrient and energy metabolism, *Molecules* (Basel, Switzerland), 24 (2019).
- [9] B. Gross, M. Pawlak, P. Lefebvre, B. Staels, PPARs in obesity-induced T2DM, dyslipidaemia and NAFLD, *Nat. Rev. Endocrinol.* 13 (2017) 36–49.
- [10] S. Francque, A. Verrijken, S. Caron, J. Prawitt, R. Paumelle, B. Derudas, P. Lefebvre, M.R. Taskinen, W. Van Hul, I. Mertens, G. Hubens, E. Van Marck, P. Michielsens, L. Van Gaal, B. Staels, PPARalpha gene expression correlates with severity and histological treatment response in patients with non-alcoholic steatohepatitis, *J. Hepatol.* 63 (2015) 164–173.
- [11] K.H. Liss, B.N. Finck, PPARs and nonalcoholic fatty liver disease, *Biochimie* 136 (2017) 65–74.
- [12] H. Kim, M. Haluzik, Z. Asghar, D. Yau, J.W. Joseph, A.M. Fernandez, M.L. Reitman, S. Yakar, B. Stannard, L. Heron-Milhavet, M.B. Wheeler, D. LeRoith, Peroxisome proliferator-activated receptor-alpha agonist treatment in a transgenic model of type 2 diabetes reverses the lipotoxic state and improves glucose homeostasis, *Diabetes* 52 (2003) 1770–1778.
- [13] Y.X. Wang, C.H. Lee, S. Tjep, R.T. Yu, J.Y. Ham, H.J. Kang, R.M. Evans, Peroxisome-proliferator-activated receptor delta activates fat metabolism to prevent obesity, *Cell* 113 (2003) 159–170.
- [14] X. Palomer, E. Barroso, J. Pizarro-Delgado, L. Pena, G. Botteri, M. Zarei, D. Aguilar, M. Montori-Grau, M. Vazquez-Carrera, PPAR beta/delta: a key therapeutic target in metabolic disorders, *Int. J. Mol. Sci.* 19 (2018).
- [15] T. Tanaka, J. Yamamoto, S. Iwasaki, H. Asaba, H. Hamura, Y. Ikeda, M. Watanabe, K. Magoori, R.X. Ioka, K. Tachibana, Y. Watanabe, Y. Uchiyama, K. Sumi, H. Iguchi,

- S. Ito, T. Doi, T. Hamakubo, M. Naito, J. Auwerx, M. Yanagisawa, T. Kodama, J. Sakai, Activation of peroxisome proliferator-activated receptor delta induces fatty acid beta-oxidation in skeletal muscle and attenuates metabolic syndrome, *Proc. Natl. Acad. Sci. USA* 100 (2003) 15924–15929.
- [16] D.L. Sprecher, C. Massien, G. Pearce, A.N. Billin, I. Perlstein, T.M. Willson, D.G. Hassall, N. Ancellin, S.D. Patterson, D.C. Lobe, T.G. Johnson, Triglyceride:high-density lipoprotein cholesterol effects in healthy subjects administered a peroxisome proliferator activated receptor delta agonist, *Arterioscl. Throm. Vas.* 27 (2007) 359–365.
- [17] T. Adhikary, A. Wortmann, T. Schumann, F. Finkernagel, S. Lieber, K. Roth, P.M. Toth, W.E. Diederich, A. Nist, T. Stiewe, L. Kleinesudeik, S. Reinartz, S. Muller-Brusselbach, R. Muller, The transcriptional PPARbeta/delta network in human macrophages defines a unique agonist-induced activation state, *Nucleic Acids Res.* 43 (2015) 5033–5051.
- [18] M. Ahmadian, J.M. Suh, N. Hah, C. Liddle, A.R. Atkins, M. Downes, R.M. Evans, PPAR gamma signaling and metabolism: the good, the bad and the future, *Nat. Med.* 19 (2013) 557–566.
- [19] G. Derosa, A. Sahebkar, P. Maffioli, The role of various peroxisome proliferator-activated receptors and their ligands in clinical practice, *J. Cell. Physiol.* 233 (2018) 153–161.
- [20] A.Z. Mirza, I.I. Althagafi, H. Shamsad, Role of PPAR receptor in different diseases and their ligands: physiological importance and clinical implications, *Eur. J. Med. Chem.* 166 (2019) 502–513.
- [21] F. Hong, P. Xu, Y. Zhai, The opportunities and challenges of peroxisome proliferator-activated receptors ligands in clinical drug discovery and development, *Int. J. Mol. Sci.* 19 (2018).
- [22] Z. Li, Z. Zhou, F. Deng, Y. Li, D. Zhang, L. Zhang, Design, synthesis, and biological evaluation of novel pan agonists of FFA1, PPARgamma and PPARdelta, *Eur. J. Med. Chem.* 159 (2018) 267–276.
- [23] Z. Li, Y. Chen, Z. Zhou, L. Deng, Y. Xu, L. Hu, B. Liu, L. Zhang, Discovery of first-in-class thiazole-based dual FFA1/PPARdelta agonists as potential anti-diabetic agents, *Eur. J. Med. Chem.* 164 (2019) 352–365.
- [24] Z. Li, L. Hu, X. Wang, Z. Zhou, L. Deng, Y. Xu, L. Zhang, Design, synthesis, and biological evaluation of novel dual FFA1 (GPR40)/PPARdelta agonists as potential anti-diabetic agents, *Bioorg. Chem.* 92 (2019) 103254.
- [25] B. Cariou, B. Charbonnel, B. Staels, Thiazolidinediones and PPARgamma agonists: time for a reassessment, *Trends Endocrin. Met.* 23 (2012) 205–215.
- [26] A.M. Lincoff, J.C. Tardif, G.G. Schwartz, S.J. Nicholls, L. Ryden, B. Neal, K. Malmberg, H. Wedel, J.B. Buse, R.R. Henry, A. Weichert, R. Cannata, A. Svensson, D. Volz, D.E. Grobbee, Effect of aleglitazar on cardiovascular outcomes after acute coronary syndrome in patients with type 2 diabetes mellitus: the AleCardio randomized clinical trial, *JAMA* 311 (2014) 1515–1525.
- [27] H.J. An, B. Lee, D.H. Kim, E.K. Lee, K.W. Chung, M.H. Park, H.O. Jeong, S.M. Kim, K.M. Moon, Y.R. Kim, S.J. Kim, H.Y. Yun, P. Chun, B.P. Yu, H.R. Moon, H.Y. Chung, Physiological characterization of a novel PPAR pan agonist, 2-(4-(5,6-methylene-dioxybenzo[d]thiazol-2-yl)-2-methylphenoxy)-2-methylpropanoic acid (MHY2013), *Oncotarget* 8 (2017) 16912–16924.
- [28] Y.-S. Lee, Y.-H. Cho, S. Lee, J.-K. Bin, J. Yang, G. Chae, C.-H. Cheon, Significant facilitation of metal-free aerobic oxidative cyclization of imines with water in synthesis of benzimidazoles, *Tetrahedron* 71 (2015) 532–538.
- [29] T. Shinozuka, T. Tsukada, K. Fujii, E. Tokumaru, K. Shimada, Y. Onishi, Y. Matsui, S. Wakimoto, M. Kuroha, T. Ogata, K. Araki, J. Ohsumi, R. Sawamura, N. Watanabe, H. Yamamoto, K. Fujimoto, Y. Tani, M. Mori, J. Tanaka, Discovery of DS-6930, a potent selective PPARgamma modulator. Part I: Lead identification, *Bioorg. Med. Chem.* 26 (2018) 5079–5098.
- [30] A. Gutierrez-Hernandez, Y. Galvan-Cipres, E. Alberto Dominguez-Mendoza, Y. Aguirre-Vidal, S. Estrada-Soto, J. Cesar Almanza-Perez, G. Navarrete-Vazquez, Synthesis design antihyperglycemic studies, and docking simulations of benzimidazole-thiazolidinedione hybrids, *J. Chem.* (2019) 1650145.
- [31] M.A. Herrera-Rueda, H. Tlahuext, P. Paoli, A. Giacomani-Martinez, J.C. Almanza-Perez, H. Perez-Sanchez, A. Gutierrez-Hernandez, F. Chavez-Silva, E.A. Dominguez-Mendoza, S. Estrada-Soto, G. Navarrete-Vazquez, Design, synthesis, in vitro, in vivo and in silico pharmacological characterization of antidiabetic N-Boc-L-tyrosine-based compounds, *Biomed. Pharmacother.* 108 (2018) 670–678.
- [32] T. Tsuchida, Y.A. Lee, N. Fujiwara, M. Ybanez, B. Allen, S. Martins, M.I. Fiel, N. Goossens, H.I. Chou, Y. Hoshida, S.L. Friedman, A simple diet- and chemical-induced murine NASH model with rapid progression of steatohepatitis, fibrosis and liver cancer, *J. Hepatol.* 69 (2018) 385–395.